molecular pharmaceutics

Article

pubs.acs.org/molecularpharmaceutics

Formulation Pre-screening of Inhalation Powders Using Computational Atom–Atom Systematic Search Method

Vasuki Ramachandran,[†] Darragh Murnane,*[,‡] Robert B. Hammond,[†] Jonathan Pickering,[†] Kevin J. Roberts,*[,†] Majeed Soufian,[†] Ben Forbes,[§] Sara Jaffari,[§] Gary P. Martin,[§] Elizabeth Collins,[∥] and Klimentina Pencheva[∥]

[†]Institute of Particle Science and Engineering, Institute of Process Research and Development, School of Chemical and Process Engineering, University of Leeds, Leeds LS2 9JT, U.K.

[‡]School of Life and Medical Sciences, University of Hertfordshire, Hertfordshire AL10 9AB, U.K.

[§]Institute of Pharmaceutical Sciences, King's College, London SE1 9NH, U.K.

[∥]Pfizer, Sandwich CN13 9NJ, U.K.

Supporting Information

ABSTRACT: The synthonic modeling approach provides a molecule-centered understanding of the surface properties of crystals. It has been applied extensively to understand crystallization processes. This study aimed to investigate the functional relevance of synthonic modeling to the formulation of inhalation powders by assessing cohesivity of three active pharmaceutical ingredients (APIs, fluticasone propionate (FP), budesonide (Bud), and salbutamol base (SB)) and the commonly used excipient, α-lactose monohydrate (LMH). It is found that FP (−11.5 kcal/mol) has a higher cohesive strength than Bud (−9.9 kcal/mol) or SB (−7.8 kcal/mol). The prediction correlated directly to cohesive strength measurements using laser diffraction, where the airflow pressure required for complete dispersion (CPP) was 3.5, 2.0, and 1.0 bar for FP, Bud, and SB, respectively. The highest cohesive strength was predicted for LMH (−15.9 kcal/mol), which did not correlate with the CPP value of 2.0 bar (i.e., ranking lower than FP). High FP–LMH adhesive forces (−11.7 kcal/mol) were predicted. However, aerosolization studies revealed that the FP–LMH blends consisted of agglomerated FP particles with a large median diameter (∼4–5 μm) that were not disrupted by LMH. Modeling of the crystal and surface chemistry of LMH identified high electrostatic and H-bond components of its cohesive energy due to the presence of water and hydroxyl groups in lactose, unlike the APIs. A direct comparison of the predicted and measured cohesive balance of LMH with APIs will require a more in-depth understanding of highly hydrogen-bonded systems with respect to the synthonic engineering modeling tool, as well as the influence of agglomerate structure on surface–surface contact geometry. Overall, this research has demonstrated the possible application and relevance of synthonic engineering tools for rapid pre-screening in drug formulation and design.

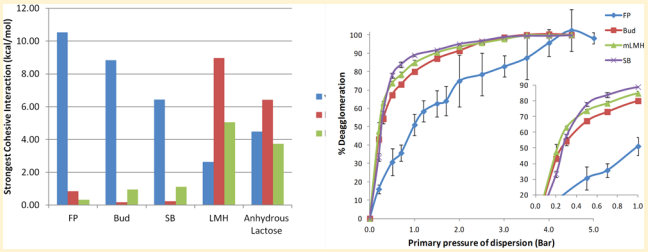

KEYWORDS: *powder dispersion analysis, in silico formulation design, inhalation drug delivery, inter-particle interaction, molecular and synthonic modeling, salbutamol, fluticasone propionate, budesonide, α-lactose monohydrate, laser diffraction, de-agglomeration*

1. INTRODUCTION

The study of interaction forces between particles in pharmaceutical formulations (e.g., active pharmaceutical ingredients (APIs) and excipients) has increased in importance over the past 20 years with the emergence of very sensitive surface analytical techniques such as atomic force microscopy (AFM) and inverse gas chromatography (IGC). Physical interaction between similar particles (e.g., API–API) is known as cohesive force,[1] and the interaction between heterogeneous particles (e.g., API–excipient) is known as adhesive force.[1] The ability to study adhesive or cohesive interactions between particles is beneficial in understanding or even predicting behaviors as diverse as blending operations[2] (and the resultant content uniformity) to tablet compaction[3,4] or disintegration,[5] where surface interactions dictate the strength of surface contacts. It is not straightforward to detect these interactions in a formulation by simple experimental techniques.

The quality-by-design (QbD) approach in pharmaceutical development is a systematic and holistic approach,[6,7] in which the compatibility test to select the right API(s)–excipient combination to deliver the critical quality attributes for the drug product is the foremost step in drug development. There is not

Received: May 6, 2014
Revised: October 31, 2014
Accepted: November 7, 2014
Published: November 7, 2014

one single effective method for compatibility testing. For example, dry powder inhaler formulations depend to some extent on one or several of the following parameters: crystallinity, water content, charge, size, shape, flow, and mechanical properties of the components of the inhaler formulation.[8−10] Therefore, a combination of the many available techniques (such as AFM, scanning electron microscopy (SEM), IGC, powder electrostatics, high-performance liquid chromatography (HPLC), Fourier transform infrared spectroscopy (FT-IR), and differential scanning calorimetry (DSC)) is generally used to test the physical stability of the formulated drug and/or the chemical compatibility of API−excipient.[11]

An understanding of inter-particulate interactions between the formulated components is of immense importance in the QbD approach. In inhaled drug delivery the small size required for particle deposition in the lung (<6 μm),[12] inter-particulate interactions originating from surface forces (van der Waals, electrostatic, and capillary forces) to dominate over gravitational forces. Micronized drug particles display highly cohesive behavior and tend to form agglomerates, which must be effectively dispersed upon inhalation to be suitable for lung deposition.[13] APIs in low-dose inhalation powders are formulated with coarse "carrier" particles, usually crystalline lactose monohydrate, which serves primarily as a diluent in the formulation. However, extensive evidence exists that the use of carrier particles also serves to improve flow, dose uniformity, dispersion, and aerosolization of otherwise cohesive particles.[14] To gain an understanding of the cohesive and adhesive interactions between APIs and excipients is therefore an important pre-formulation requirement in inhaled drug delivery.

SEM, IGC, AFM, and electrostatics techniques have emerged as the most popular methods to gain some understanding of the static and dynamic API−excipient interactions.[9,11] Although suitable for use as complementary techniques to aid in probing inter-particle interactions, they are not able to directly predict strength and surface specificity of API−API and API−excipient interfacial interactions. The tensile strength and AFM methods of measuring adhesion force[15] are susceptible to inconsistency due to sample preparation, surface roughness, and surface chemistry that affect the type and orientation of the functional groups interacting at the contact points of both surfaces. The cohesive−adhesive balance (CAB) model based on AFM measurements[2] provides a quantitative method to predict the strongest inter-particle forces present, i.e., the cohesive force or the adhesive force in an API−excipient pair. The method allows predictive ranking of adhesive behavior to understand the mixing, blending, and aerosolization behavior of inhalation blends of micronized APIs with lactose.[1,16] However, the technique is not trivial to perform and is still dependent on the contact area and geometry of the probes and crystal faces under study, as shown by James and co-authors.[17]

Surface energy measurements using IGC have been particularly useful in improving our understanding of the crystallinity and surface properties of micronized particles.[18,19] Particularly, new-generation surface energy analysis (SEA)[20,21] is effective at characterizing the surface energy of micronized particles, including the dispersive and specific components of crystal surface free energy. Therefore, IGC is useful for assessing the interaction forces between particles,[22,23] including cohesive and adhesive interactions of blended particles, and for predicting dry powder inhaler performance.[24] SEA is often used in combination with other techniques (similarly to CAB modeling using AFM). Whereas AFM measures adhesive force, but only for several isolated (and hopefully representative) particles, IGC/SEA examines more representative surface areas of bulk powders, but it does not measure actual inter-particulate contact forces. Both techniques are time-consuming and may not be cost-effective, especially at the pharmaceutical research and development stage, where material availability is typically low.

Laser diffraction studies provide a method to measure the agglomeration state of particles in formulations and have been used to investigate the aerosolization potential of suspended APIs[25] as well as dry powder inhalation systems. Rapid screening tests have been proposed to characterize the de-agglomeration (in terms of the cohesive forces)[26,27] of particles from the critical pressure that is required to disperse particles of certain size through laser diffraction techniques. Although laser diffraction methods require reasonably large amounts of sample, they do serve to examine materials in a manner that is representative of in-use powder behavior and may probe blend structure.[28]

Thus far, all major methods for studying the forces of interaction between particles in inhalation powder systems have disadvantages. In particular, many of the methods must be used in tandem with each other and are time-consuming or material-expensive. The *in silico* model applied in this research adopts a "synthonic engineering approach" as a pre-screening formulation design tool through the quantitative evaluation of the interactions between molecular building blocks or functional groups known as synthons. The balance between the intrinsic synthons (fully coordinated interactions within the bulk crystal lattice) and the extrinsic synthons (interactions giving rise to unsaturation at the interface with the solvent or excipient(s)) provides an understanding of the complex surface properties and, in general, the likely formulation behavior. *In silico* predictive tools have not been widely employed so far beyond specialist groups, but they offer an attractive alternative in terms of predicting particle formation[3,29] and have found application in morphological prediction,[30] salt/co-crystal former selection,[31] inter-particle interactions,[32,33] and nucleation control of polymorphic forms.[34] In the current research, the synthonic molecular modeling tool using the grid search method is applied to examine the extrinsic synthons involved in molecule/surface binding in order to get an understanding of the inter-particle interactions that underpin the agglomeration and aerosolization behavior in inhaled formulations. This method has potential to offer a robust and effective screening approach or compatibility test to pre-select likely API−excipient combinations and, through this, to reduce the range of formulation that must be assessed using conventional laboratory techniques. The case study systems include an excipient, α-lactose monohydrate (LMH), and three APIs, salbutamol (SB), fluticasone propionate (FP), and budesonide (Bud). The prediction work is validated through independent experimental de-agglomeration studies using laser diffraction techniques.

2. SYNTHONIC MODELING

Crystallization is the primary method used by the pharmaceutical industry in the isolation and purification of APIs from the upstream synthesis environment. In addition to facilitating the formation of crystalline particles, the nucleation and growth stages of the crystallization process can pre-configure a number

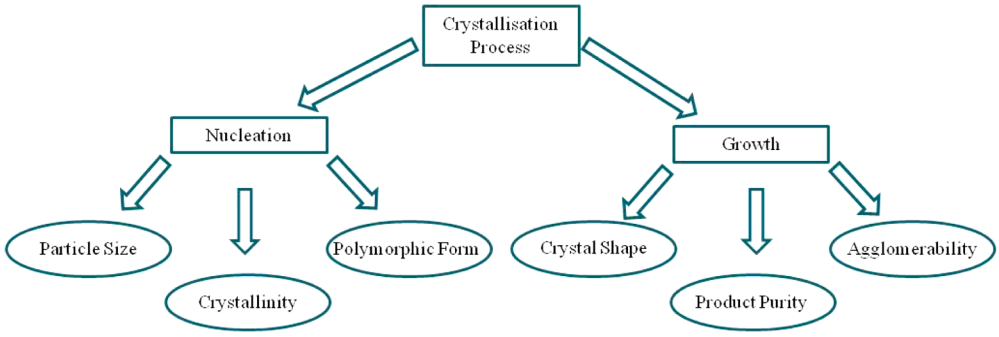

Figure 1. Schematic showing the role played by the functional parameters of crystallization (nucleation and growth) in directing the physical properties of solid forms that result. Prediction of the outcomes would allow greater control of the final product.

of the key physicochemical properties that are important in the utility and performance of drug products downstream (see Figure 1). In this schematic, nucleation refers to the bulk nucleation, which is a three-dimensional process having an effect on the bulk properties, such as size, polymorphism, and mechanical properties, while the two-dimensional crystal growth process has an effect on the crystal shape and agglomeration. Knowledge of the inter-molecular interactions, in aggregate referred to as synthons, involved in crystal formation can help us understand, predict, control, and scale-up crystallization processes. Such details can be derived from the crystallizing material's crystallographic structure using molecular modeling techniques.

The synthons mostly consist of isotropic van der Waals and electrostatic interactions between inter-molecular atom pairs, together with highly directional H-bonds. The synthons—in particular, the extrinsic synthons—are important in that they can potentially have a significant impact on the physical and chemical properties of a crystalline particle, e.g., relative crystal growth rate, particle shape, reactivity, agglomerability, etc. Synthonic analysis requires knowledge of the basic chemistry of the molecules together with details concerning the crystal lattice and its associated inter-molecular arrangement. Although such supramolecular science is reasonably well-established, the manipulation of synthonic interactions in a manner analogous to that used in chemical (molecular) synthesis has received little attention in recent years. Synthonic engineering thus provides the opportunity to exploit synthon directionality and energetic to understand, design, and potentially control the physicochemical properties of such molecular assemblies. The latter is helpful as it enables prediction of product- and quality-related properties *in silico*, this reducing, in principle, the need for lengthy and expensive experimental studies.

2.1. Bulk (Intrinsic) Interactions. Habit comprises a lattice-energy calculator and energy-based morphology predictor. Habit analyzes the magnitude of the ratio of the extrinsic synthons to the intrinsic synthons of the bulk structure. Comparing the values obtained for different crystal faces can, e.g., be used to predict the external morphology. These calculations require knowledge of the crystal system, the chemistry of the molecules, and a suitable inter-atomic potential. Essentially the approach is to sum the inter-atomic potential for all the molecules within a given limit of a central molecule, to produce a molar lattice energy value. Habit has the following key features:

- Calculate the strength and direction of the inter-molecular interactions in a crystal structure, providing also an analysis of the local coordination sphere around a targeted central molecule.
- Calculate the lattice energy of a fully extended organic crystal structure and the same for molecular clusters as a function of their size and shape. Calculations on many structures may be carried out in batch mode, with the results written to spread-sheet readable files.
- Display the lattice energy convergence as a function of the limiting range of the calculation.
- A choice of potentials (force fields).
- Calculate the surface attachment energy for any plane defined by its Miller indices.
- Visualize the morphology and calculate the percentage surface areas of the simulated morphological forms, the surface/volume ratio of the particle, and the diameter of its spherical (volume or surface area) equivalent diameter.

2.2. Surface (Extrinsic) Interactions. SystSearch is a simulator which predicts the interaction of the crystal surfaces with the external environment. SystSearch analyses the extrinsic synthons and uses a systematic grid-based search to calculate the possible interaction energies between a probe molecule and another molecule or with a crystal surface. The probe molecule can itself be configured as a surface, thus enabling the interactions between two surfaces to be probed. This approach has been used to model the morphology of crystals as a function of solvent type and/or different additive species as well as to assess the energetics of putative inter-molecular interactions, such as the molecular pairs associated with salt and co-crystal former selection as well as inter-particle surface match associated with solvent-mediated polymorphic transformations and API−excipient interactions. This requires the same information as Habit plus additional information on the structure and chemistry of the probe. SystSearch has the following key features:

- The interaction energy is calculated for the chosen surface of the crystal structure and the selected probe molecule by a grid search of possible configurations of the molecule relative to the surface. Suitable search parameters are provided by default.
- There is an option to display the geometrical configuration information which enables an advanced user to modify the search parameters.
- The output is displayed as a data window which can be manipulated to visualize the most stable interaction energy using a histogram, or the statistics of mean, sum, or mode of the interaction energy, or energy iso-surfaces

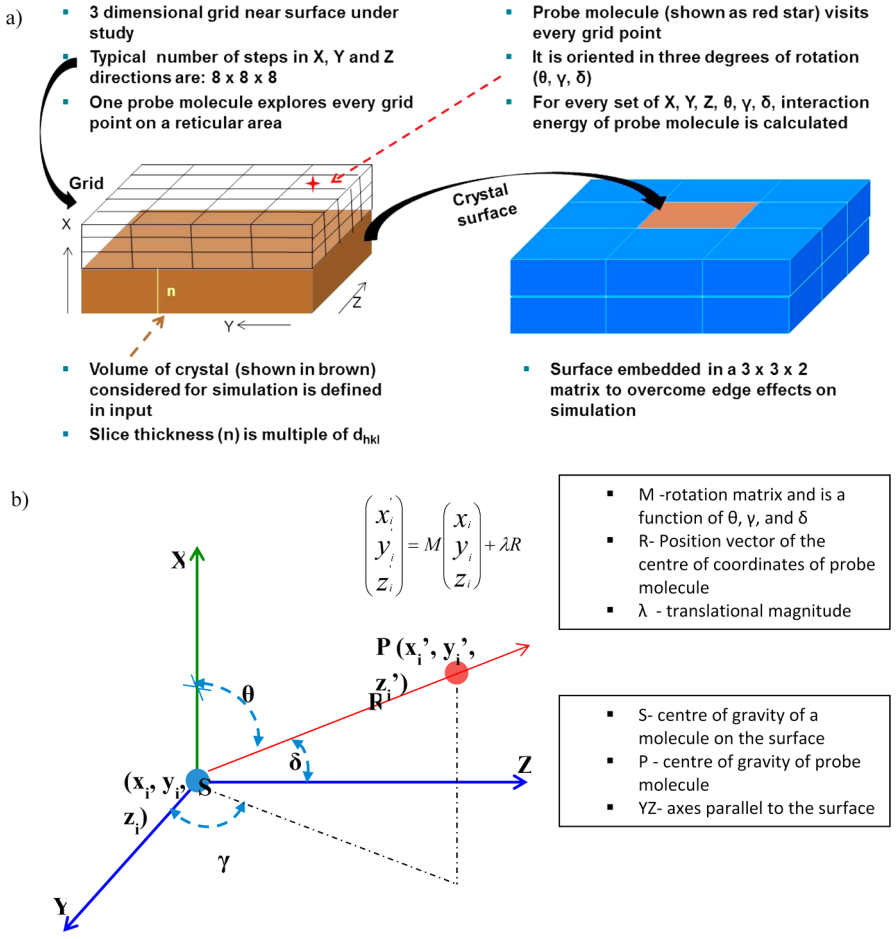

Figure 2. Schematic representation highlighting the main computational methodology associated with the systematic search. (a) Probe molecule in the context of the surface and the virtual grids. (b) Cartesian coordinates of the probe molecule with respect to a molecule on the surface with which it is interacting.

(contour-plot) of the number of binding sites as a function of their interaction energy.

3. MATERIALS AND METHODS

3.1. Materials. The materials considered for this study are α-lactose monohydrate and three APIs, salbutamol, fluticasone propionate, and budesonide. The crystal structures of these materials (LACTOS11,[35] BHHPHE,[36] DAXYUX,[37] and SHBUXP10[38]) are taken from the Cambridge Structural Database (CSD) for the *in silico* study.

The suppliers of the above materials for the experimental work were as follow: budesonide (Bud; LGM Pharma, USA, batch no. U0015/1V040), fluticasone propionate (FP; LGM Pharma, USA; FP1, batch no. 458763; FP2, batch no. 5501-B-11030), Lactohale 300 (mLMH; Frieslands Foods, Domo, The Netherlands; batch no. 6125224/S), salbutamol base (SB; Pharm Dev Europe; GWRD, batch no. WC46269), lactose monohydrate (coarse grade, cLMH; Pfizer Ltd., Sandwich, UK; batch no. 120904-25).

3.2. Computational Method. The molecular and synthonic modeling approach has two component parts: prediction of crystal habit based upon the crystallographic structures, and prediction of the cohesive/adhesive energies. The molecular modeling approach has two parts: prediction of crystal habit, followed by *in silico* prediction of the cohesive/adhesive energy. The prediction of crystal habit from the crystal structure is based on an atomistic approach which has been explained elsewhere.[39] The crystal habits for all the materials are predicted using the attachment energy model. The attachment energy (E_{att}^{hkl}) is the measure of the energy released on addition of a growth slice (hkl) to the growing crystal, and is directly proportional to its relative growth rate (R^{hkl}) normal to the surface (hkl). Attachment energies are calculated for all the materials examined using Habit98,[40] and hence the crystal habit is predicted. Crystal faces with smaller absolute values of attachment energy are slower growing and have larger relative surface areas; i.e., they become morphologically dominant

3.2.1. Molecule/Surface Binding. The surface packing diagrams are generated by the Accelrys software, Materials Studio version 6.0.[41] The intra- and inter-molecular H-bonds are denoted as blue broken lines in all the figures. All the surfaces denoted by white lines are cleaved from the crystal with one d-spacing deep. The most important surfaces from the predicted habit were, in turn, selected as the substrate for the prediction of the adhesive/cohesive interactions of probe molecules onto the crystal habit surfaces. This was carried out using the SystSearch which utilizes a grid-based, systematic search. This systematic search application is an extension to the approach already applied in a molecular-pair model[31] and a cluster-pair model.[33] The current modeling approach generates an atomistic model of a specific crystalline surface, with a well-defined termination which retains complete molecules in the host surface, and enables a probe molecule to explore the

dx.doi.org/10.1021/mp500335w | *Mol. Pharmaceutics* 2015, 12, 18−33

energy landscape as it interacts with the surface. The probe molecule can either be an excipient molecule or an API molecule, and similarly, the surface can either be an excipient crystal surface or an API crystal surface, thus allowing cohesive and adhesive interactions to be quantified. The host crystal structure is optimized with respect to the Dreiding force field,[42] but the surface is not relaxed further during the systematic search by the probe. In all the systematic searches, a slice thickness of 2 times the inter-planar spacing for the surface (hkl) is chosen. A three-dimensional virtual grid is generated adjacent to the crystal-surface model as shown in the schematic in Figure 2a. A probe molecule, treated as a rigid body, visits every grid point in turn and is orientated, sequentially, in one of a specified number of orientations. The in-plane dimensions of the search space are periodic (several reticules) but non-periodic in the direction normal to the crystal surface. Reticular area is a projection of the unit cell on a surface plane. Reticular area (S_{hkl}) is calculated from the ratio of the unit cell volume (V_{cell}) to the d-spacing (d_{hkl}) as shown in eq 1.

$$S_{hkl} = \frac{V_{cell}}{d_{hkl}} \tag{1}$$

The search area is further divided into grids defined by the step size for the translational movement as well as the orientation of the probe. Generally, the total number of grid points in the search space is held constant for a set of related searches. In the in-plane y- and z-directions the step sizes are expressed in fractional coordinates and relate to the cell axes in-plane, i.e., the axes which define the reticule. In the direction perpendicular to the plane the interval between adjacent grid points is expressed in units of angstroms. The typical value of the step size for the parameters that define the orientation of the probe molecule is set to 30°. Orientation is defined with respect to the principal axes of the probe molecule which are calculated from the Cartesian coordinates of the constituent atoms without applying mass weighting. A pairwise atom−atom interaction energy is calculated between the probe molecule, at the center of a sphere with a cutoff radius of 25 Å, and every molecule in the surface slab within the sphere. The Cartesian coordinates of the center of gravity of the probe molecule is explained in Figure 2b. Interaction energy is calculated for every grid point location and at that location for all the specified orientations of the probe molecule. The program is capable of listing various statistics such as mean, minimum, total, mode, distribution, number of favorable sites, etc. from these calculations.

The most energetically favorable location and orientation of the isolated probe molecule on the crystal surface were identified. Currently the position and orientation of the probe are not subsequently optimized with respect to the pairwise interaction energy. The simulations to predict the cohesive interaction of the three API systems (SP, BUD, SB) are carried out with one molecule of the API on all the surfaces of its crystal. In the case of LMH, one molecular pair of lactose and water is treated as the probe on all the surfaces of the LMH crystal.

The technique is robust and simple to use; however, it is important to note that the method is based on some assumptions, as follows:

- The model calculates and predicts the interaction between a single molecule and a crystal surface and does not take cluster−cluster interaction into consideration.
- The crystal lattice is perfect and devoid of any defects.
- Interactions between another molecule and/or other heterogeneous species are not taken into account.
- The surface can be represented by a termination of the bulk lattice, and there is no surface reconstruction.
- The probe molecule is treated as a rigid body in the grid search, and the conformational change due to surface interactions is not taken into account.
- The growth solvent effects are not explicitly taken into consideration, i.e., equivalent wetting of the surfaces with respect to the solid−solid, solid−fluid, and fluid−fluid inter-molecular interactions for all the crystal faces.
- The model does not take into account the probe charging effects, i.e., due to speciation.

3.3. Experimental Method. The powder blends were prepared for experimental assessment of cohesive energy analysis, dispersive surface energy measurements using IGC, and aerosolization characterization.

3.3.1. Production of Mixed Powder Blends. Binary fine particle blends were prepared consisting of FP1 and mLMH (blend size 1 or 3 g, ratio 1:4, and 1 or 5 g, ratio 1:8 w/w in 15 and 100 mL glass bottles, respectively). Blending was by geometric mixing, where drug and lactose were added sequentially in approximately equal volumes to the powder already contained in the mixing vial. Following each addition, the blending vessel was placed on a vortex mixer and subjected to agitation for 60 s, followed by 60 s of stirring with a spatula to break up any large agglomerates. Up to three ceramic beads (approximately 10 mm diameter) were added to the vessel for 1 and 3 or 5 g blends, respectively, and the blend was tumbled using a shaker mixer at 62 rpm for 40 min. As controls, FP1 and mLMH were subjected to a tumbling process similar to that used for the mixtures prior to aerosolization assessment.

A similar process was followed for blends of FP2 with coarse-grade lactose (cLMH, blend size 3 g, 1.4% w/w), with the exceptions that the blending was performed in 15 mL glass vials, the blends were not manually triturated with a spatula, and two 10 mm diameter ceramic beads were employed. Blends were stored in a desiccator over dry silica before use. Content uniformity analysis involved assessing drug recovery ($n \geq 6$) using validated HPLC methods. No blend was examined further unless the coefficient of variance of drug content was <6%.

3.3.2. Measurement of Powder Cohesion Using Dry Powder Laser Diffraction Analysis. Laser diffraction analysis was performed using a Sympatec HELOS/RODOS instrument with a rotary feeder dispersion unit (Sympatec GmbH, Clausthal-Zellerfeld, Germany) using an R3 lens (0.9−175 μm), with a forced stability of 4, according to the analytical method previously reported.[27] By varying the partial pressure (PP) drop across the dispersion line in the range 0.2−5.0 bar, the degree of agglomeration (DA) was determined by normalizing the median particle size measured at each PP (eq 2):

$$\mathrm{PP} = \frac{D_m}{D_x} \times 100 \tag{2}$$

where D_m is the particle size at the maximum PP (i.e., maximum dispersion force), representing the median particle diameter at full dispersion, and D_x is the median diameter at

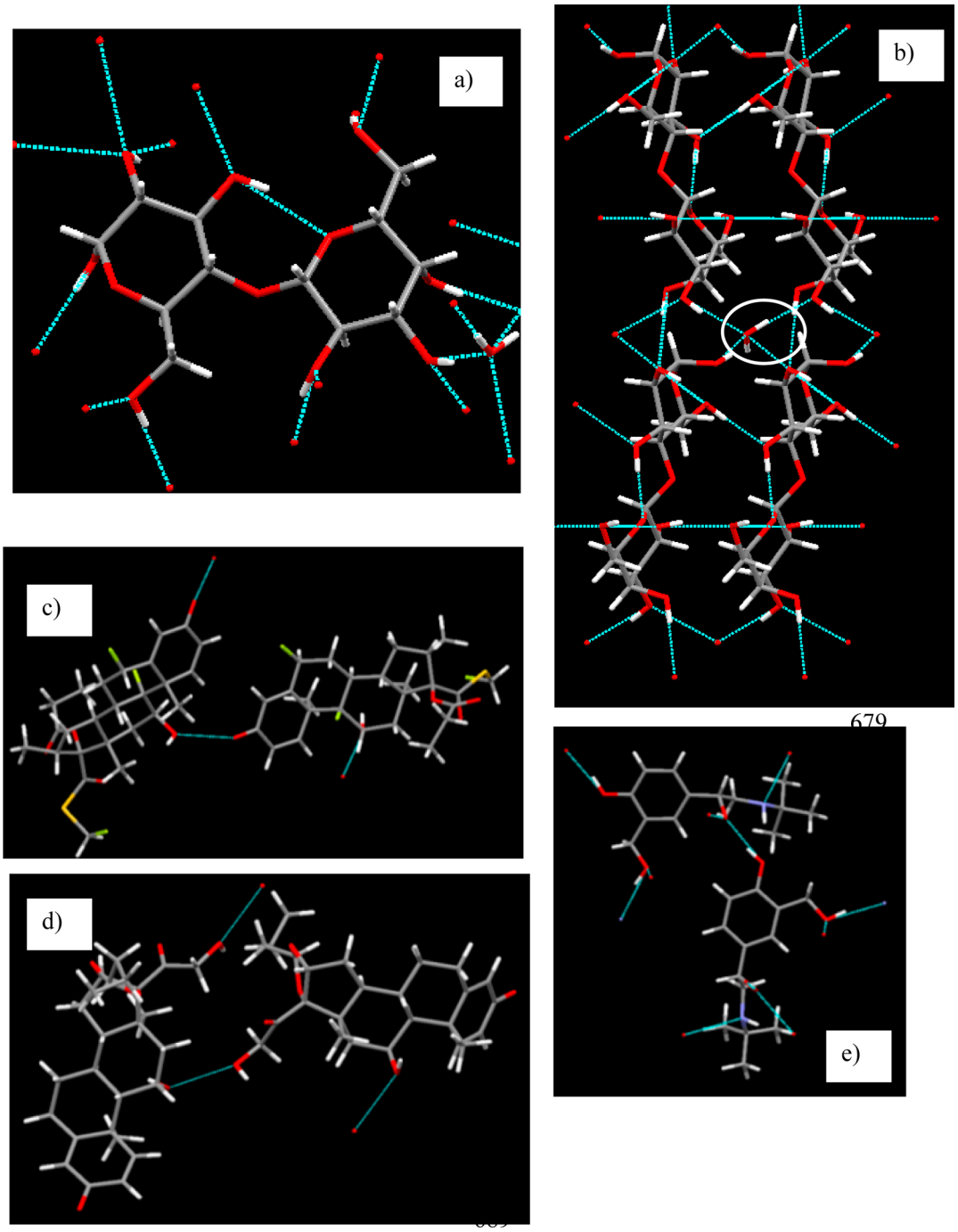

Figure 3. Molecular packing of α-lactose monohydrate. (a) A pair of lactose and water molecules with their the H-bonding donor and acceptor atoms. (b) A water molecule is connected to four lactose molecules through inter-molecular H-bonds. Color code: gray, carbon; red, oxygen; white, hydrogen; broken blue lines, H-bonds; white circle, water molecule. (c–e) Molecular packing diagrams showing the H-bonds formation in pairs of FP (c), BUD (d), and SB (e) molecules. Color code: gray, carbon; red, oxygen; white, hydrogen; blue, nitrogen; green, fluorine; yellow, sulfur; broken blue lines, H-bonds.

any other PP. The de-agglomeration curves were analyzed to calculate the critical primary pressure (CPP) and pressure required for 50% de-agglomeration (DA_{50}) as reported previously.[27]

3.3.3. Surface Energy Determination by Inverse Gas Chromatography. A 30 cm silanized glass column with an internal diameter of 3 mm was filled with 200–300 mg of sample (FP1, FP2, mLMH, and carrier lactose (cLMH)) and sealed at each end with silanized glass wool. Samples were analyzed using an SMS surface energy analyzer (SMS Ltd., London, UK). The columns were conditioned under dry helium for 2 h at 0% relative humidity (RH), using helium as carrier gas at 303 K. The probe and column temperature were set at 303 K, and analysis was conducted at 0% RH using a total flow of 10 sccm (standard cubic centimeters per minute) during conditioning and analysis cycles. The specific surface area of each sample was first determined by measuring the octane adsorption isotherms at 30 °C and 0% RH using the SEA. The BET specific surface areas of the samples were subsequently calculated from the corresponding isotherms,

dx.doi.org/10.1021/mp500335w | *Mol. Pharmaceutics* 2015, 12, 18–33

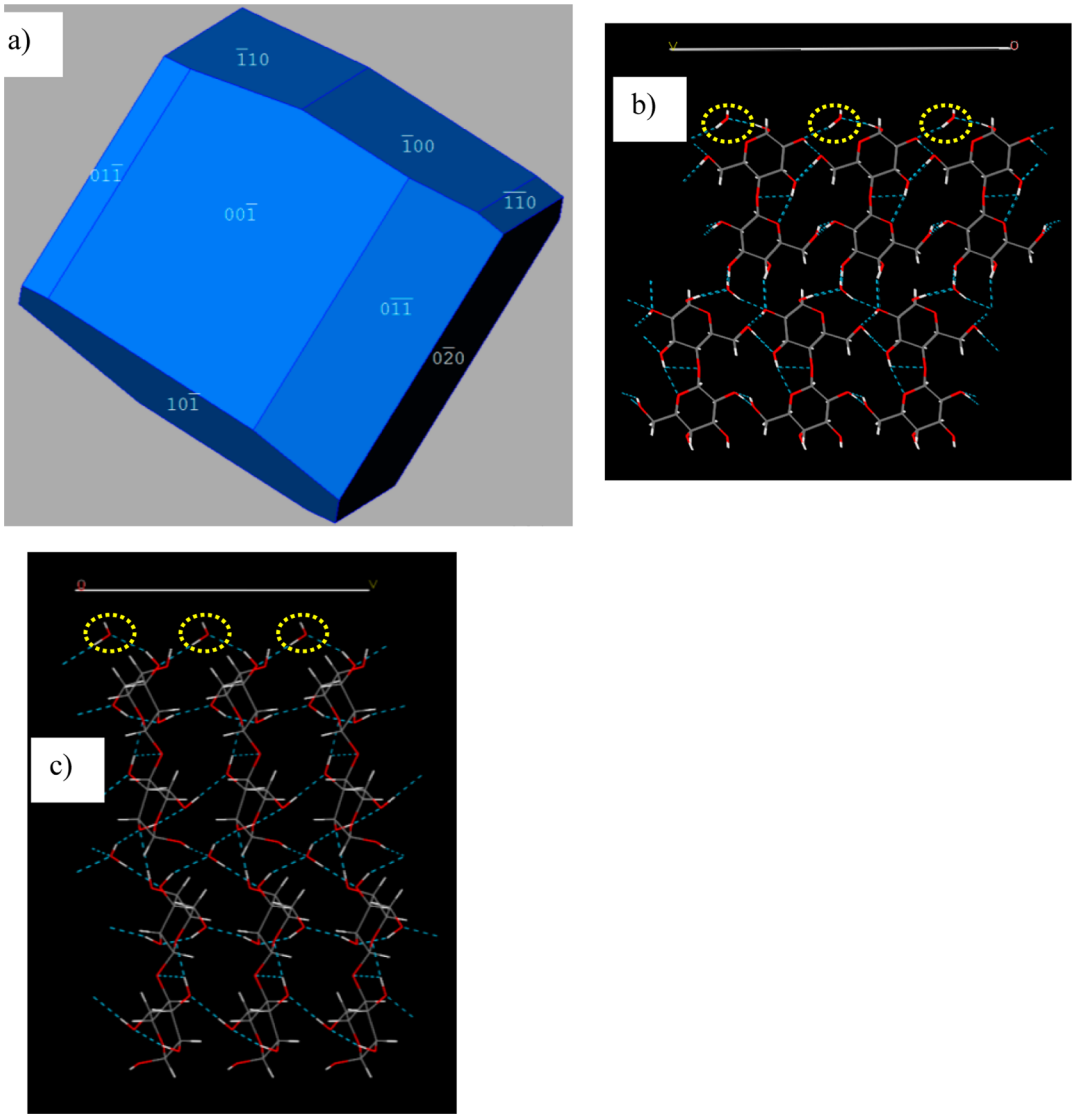

Figure 4. Predicted morphology and surface chemistry of LMH. (a) Crystal morphology as predicted by Habit. (b) Surface chemistry of LMH at the $(0\bar{2}0)$ surface, which contributes to about 17% of the total crystal surface. (c) Surface chemistry of LMH at the (020) surface, which contributes to 17% of the total crystal surface, showing the molecules forming a zigzag pattern in a direction perpendicular to the surface; the water molecules shown in yellow circles are very close to the surface.

within the partial pressure range of 5−35% P/P_0. The surface coverage (n/n_m, i.e., ratio of the amount of adsorbed gas to the BET monolayer adsorbed capacity) at each injection concentration could then be calculated from the amount adsorbed (n), obtained from integration of the net retention volume (V_N), versus the equilibrium partial pressure (P/P_0) of each injection (where P and P_0 are the equilibrium and saturated pressure of the adsorbate at the test temperature). The dead time was calculated using methane, and the surface coverages employed for surface energy determinations were in the range 0.005−0.02 n/n_m. The non-polar probes employed were nonane, octane, heptane, and hexane, and dispersive surface energy was determined using the Shultz method.[43] In addition to the non-polar probes, a range of polar probes were employed (ethanol, acetone, ethyl acetate, acetonitrile, and dichloromethane) to determine the specific (polar acid−base) surface energy components of these materials. The polar probe data were added to the Schultz plot, and the vertical distance of the data points from the alkane line was taken as equal to the specific free energy of adsorption (ΔG^{SP}) arising due to polar interactions with the sample material. The work of cohesion and adhesion was calculated following the van Oss method after Traini et al.[44]

3.3.4. Aerosolization Studies. Aerosolization performance was assessed for FP−mLMH and FP−cLMH blends according to pharmacopoeial methods. Size 3 gelatin capsules (Pfizer Global R&D, UK) were filled with 15 ± 2 or 12.5 ± 0.5 mg of blend, respectively, and an appropriate number of capsules actuated in order to achieve sufficient drug deposition within the next-generation impactor (NGI, Copley Scientific Ltd., Nottingham, UK). The impactor plates were coated with a thin layer of 11% w/v polypropylene glycol dissolved in hexane by swirling the solution around the plates and leaving them to air-dry. The NGI was assembled with 15 mL of mobile phase accurately pipetted into the pre-separator. The airflow through the NGI was set at 60 L/min ± 5% (or 1.4 kPa) across the monodose inhaler, with a total airflow of 4 L drawn through the inhaler for each capsule actuated.

dx.doi.org/10.1021/mp500335w | *Mol. Pharmaceutics* 2015, 12, 18−33

Table 1. Percentage Surface Areas of Individual Faceted Faces (Multiplicity Is Not Taken into Consideration) of the Predicted Morphology of LMH, FP, BUD, and SB (M Refers to the Multiplicity of a Face)

LMH			FP			BUD			SB		
face	% surface area	*M*	face	% surface area	*M*	face	% surface area	*M*	face	% surface area	*M*
(020)	16.5	1	(200)	15	2	(002)	20.9	2	(200)	20.5	2
(0$\bar{2}$0)	17.2	1	(110)	12.2	4	(101)	5.7	4	(002)	4.7	2
(001)	8.6	2	(101)	4.6	4	(011)	7.4	4	(111)	3.4	8
(011)	1.6	2	(011)	0.8	4	(110)	1.4	4	(102)	5.1	4
(100)	5.7	2							(210)	0.6	4
(10$\bar{1}$)	2.4	2									
(110)	2.4	2									
(1$\bar{1}$0)	1.1	2									
(0$\bar{1}$1)	5.3	2									

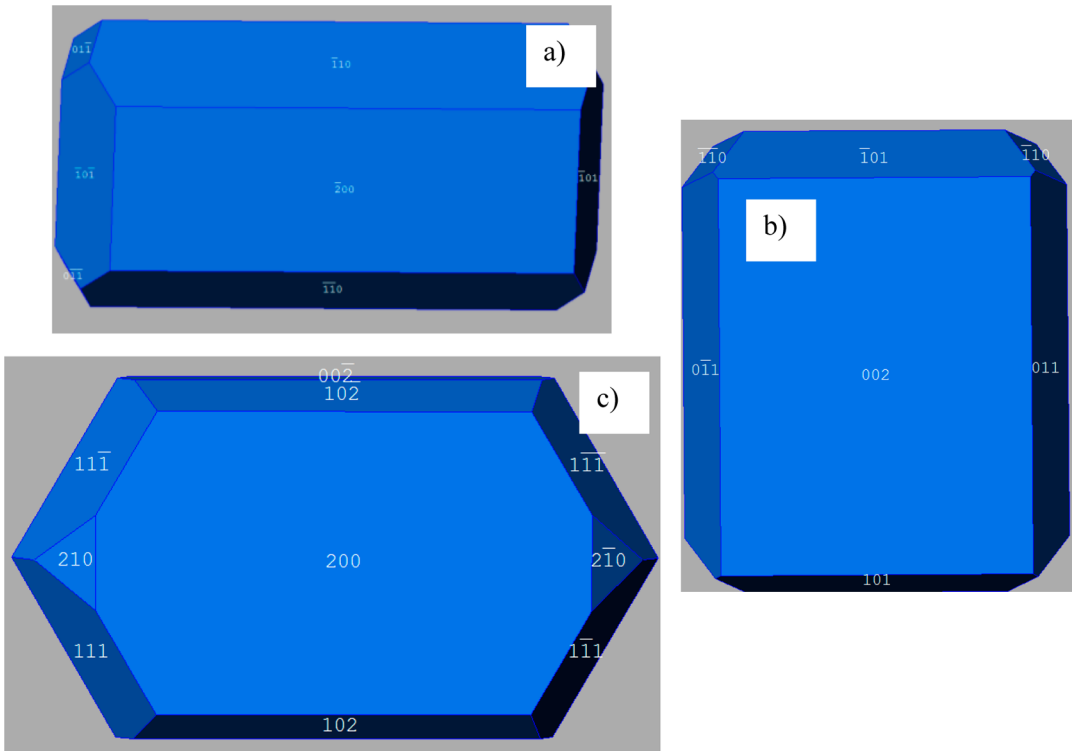

Figure 5. Predicted morphologies of APIs. (a) Fluticasone propionate with (110) facets as the most dominant and (011) as the least dominant surface. (b) *sec*-Budesonide with (002) as the dominant faces and (110) as the smallest faces. (c) Salbutamol with the dominant (200) faces and the smallest (210) faces.

The device and capsules were carefully rinsed with appropriate volumes of washing solvent (range: 20−50 mL) to collect the drug deposited, ensuring complete dissolution of recovered drug particles. The NGI induction port and pre-separator were rinsed with 50 and 100 mL of washing solvent, respectively. NGI plates 1−5 were washed with 10 mL of washing solvent, and stages 6−8 were washed with 5 mL of washing solvent, in both cases by accurate pipet transfer. A sample of each solution was withdrawn for analysis by HPLC according to a validated method for FP.[45] The washing solvent was the HPLC mobile phase, a 75:25 (v/v) mixture of methanol and 0.6% w/v aqueous ammonium acetate. Fine particle fractions (FPFs) were defined for the mass of deposited particles with a size less than 5 μm depositing in the NGI, and the mass median aerodynamic diameter was calculated by interpolation of the cumulative undersize particle distribution in accordance with British Pharmacopoeial methods.

4. RESULTS AND DISCUSSION

Results from the *in silico* studies are given in sections 4.1−4.3, and the results from the experimental methods are included in sections 4.4−4.6

4.1. Crystal Chemistry. The molecular chemistry of all the case study systems is shown in Figure 3. The donor and acceptor atoms forming the intra- and inter-molecular H-bonds are shown as broken blue lines. The hydrogen-bonded network is generated with the Cambridge Crystallographic Database Software, Mercury.[46]

The excipient, α-lactose monohydrate (LMH), is a strongly hydrogen-bonded system, as can be seen in Figure 3a. The pair of lactose and water molecules together forms 15 inter-molecular H-bonds with the neighboring lactose and water molecules and at least one intra-molecular H-bond. Every water molecule connects four lactose molecules through the H-bonds

dx.doi.org/10.1021/mp500335w | *Mol. Pharmaceutics* 2015, 12, 18−33

Table 2. Cohesive Energy Prediction from Synthonic Modeling Using the Minimum Interaction Energy

FP		Bud		SB		LMH	
form	strongest (minimum) interaction energy (kcal/mol)	form	strongest (minimum) interaction energy (kcal/mol)	form	strongest (minimum) interaction energy (kcal/mol)	form	strongest (minimum) interaction energy (kcal/mol)
{200}	−12.96	{002}	−8.69	{200}	−7.75	{020}	−17.32
{110}	−9.26	{101}	−10.75	{002}	−7.62	{001}	−15.64
{101}	−13.22	{011}	−9.27	{111}	−7.73	{011}	−14.24
{011}	−10.61	{110}	−11.11	{102}	−8.34	{100}	−16.81
				{210}	−7.44	{10$\bar{1}$}	−14.51
						{110}	−16.23
						{0$\bar{2}$0}	−14.66
						{0$\bar{1}$1}	−14.66
average	**−11.51**		**−9.96**		**−7.77**		**−15.85**

(Figure 3a). The APIs, FP, Bud, and SB, form two, two, and six inter-molecular H-bonds, respectively (Figure 3c−e).

4.2. Prediction of Morphology, and Surface Chemistry. The predicted morphology of LMH is given in Figure 4. The percentage of each of the faceted faces over the total surface area is given in Table 1, and from this table, it is understood that (0$\bar{2}$0) and (020) contribute the most to the total surface area of the predicted crystal morphology (17% each) and (1$\bar{1}$0), with the least surface area (2%) of the predicted morphology. The surface chemistry of the dominant faces is shown in Figure 4b,c. It is seen that both surfaces are hydrophilic in nature, with the presence of water molecules (shown in yellow circles) close to the surface. The molecular packing arrangements are different at these two surfaces, confirming that LMH is a polar crystal; i.e., molecules are arranged like a net in the plane below the (0$\bar{2}$0) surface (Figure 4b), and the molecules form zigzag columns below the (020) surface (Figure 4c). It should be noted that the predicted morphology of LMH is from the classical attachment energy calculations, where the same atomic charges are assigned to the molecules in the bulk as well as the surfaces. However, for the prediction of polar morphology (which is not shown here), two different sets of charges need to be assigned, i.e., to the bulk molecules and to the oncoming molecules forming the surfaces. The molecular packing diagrams of the other surfaces are provided in the Supporting Information. The predicted morphologies of the three APIs are shown in Figure 5a−c, and the percentage facet areas are listed in Table 1. The (110) surfaces contribute the most to the total surface area of FP (∼49%), followed by (200) surfaces (30%) . From the calculated percentage surface areas of BUD, it is noted that the (002) surfaces are the dominant surfaces (∼42%), whereas the (110) surfaces contribute the least (∼6%) to the total surface area of the crystal morphology. Similarly, from the surface areas of the individual faces of the predicted morphology of SB, it is seen that the (200) surfaces contribute the most (∼41%), followed by the (111) surfaces (∼27%), with (210) surfaces contributing the least (∼2%) to the total surface area of the crystal morphology.

4.3. Prediction of the Cohesive and Adhesive Interaction Using the *in Silico* Model. The minimum interaction energy between a probe molecule and a surface is the strongest interaction or the most stable (preferred) interaction energy. Table 2 shows the strongest (minimum) interaction energies of each of the probes on their respective crystal surfaces. These values are averaged over all the surfaces of the crystal. The cohesive strength is stronger if the calculated value is more negative. On this basis, it can be seen that among the APIs, FP is the most cohesive, followed by Bud and SB. However, LMH or lactose molecule on its own as the probe results in higher cohesive strengths than any API particle (Table 2). The reason for this probably reflects the fact that the solid-state chemistry of LMH is dominated by an extensive network of strong and highly directed inter-molecular H-bonds, and the contribution from these to the inter-particulate forces was computed to be a significant component of the cohesive interactions (see Figure 6) These show the absolute values of

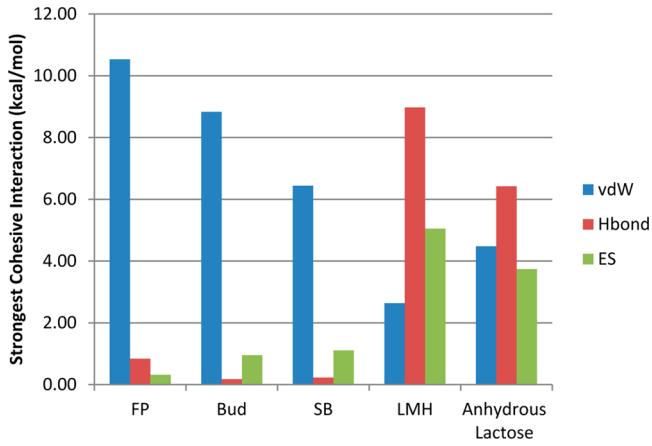

Figure 6. Breakdown of cohesive energy showing that, in LMH and anhydrous lactose, a high percentage of cohesive interaction comes from the inter- and intra-molecular H-bonds and the electrostatic contribution when compared to the APIs.

interaction energies in this cohesive interaction, whereas in the APIs the contribution of the isotropic van der Waals interactions are much higher than the electrostatic or the hydrogen-bonded contributions. The important contribution of polar interactions in defining cohesion of LMH has been reported previously using IGC,[47] which revealed that the polar surface energy was almost 3 times higher than the dispersive surface energy. Thus, the order of cohesive strength is (more negative to less negative) FP > Bud > SB. The adhesive strengths of FP on eight LMH surfaces were predicted in the same way as the cohesive strengths. The average adhesive energy of FP with LMH is very similar to the FP/FP cohesive energy (Table 3).

dx.doi.org/10.1021/mp500335w | *Mol. Pharmaceutics* 2015, 12, 18−33

Table 3. Adhesive Energy Prediction from Synthonic Modeling Using the Minimum Interaction Energy for FP on α-Lactose Monohydrate

face	strongest energy (kcal/mol)
(110)	−12.47
(100)	−13.13
(1$\bar{1}$0)	−13.33
(020)	−11.27
(011)	−11.19
(10$\bar{1}$)	−9.53
(001)	−12.00
(0$\bar{1}$)	−10.63
average	**−11.69**

4.4. Measurement of Powder Cohesion Using Dry Powder Laser Diffraction Analysis. Powder dispersibility and de-agglomeration efficiency were assessed for the micronized pure materials (Figure 7) and blends of mLMH−FP1 using laser diffraction analysis. Figure 7 presents the de-agglomeration curves for SB, mLMH, FP, and Bud, which demonstrated a range of powder de-agglomeration and dispersion behaviors. Due to the large carrier size of the FP−CL blends, it was inappropriate to apply the de-agglomeration analysis[27] to these blends. Instead, the efficiency of dispersal and de-agglomeration was assessed by impaction analysis. Laser diffraction analysis has been demonstrated to be a useful technique for characterizing the aerosolization behavior of a number of particles for inhalation.[22] The technique has several limitations, as previously reported, including the possible fragmentation of particles under the dispersion pressure, high limits of detection for the presence of particles in the laser beam, the sensitivity of the instrument to vibration, and, because it is a volumetric technique, the potential for a small number of large agglomerates to skew the estimation of de-agglomeration. Nevertheless, laser diffraction offers benefits in estimating inter-particulate cohesion. The method does not require powder pre-conditioning (unlike powder rheometry and shear cells); it is an ensemble powder technique capable of studying large numbers of particles in a powder bed (unlike AFM). Finally, the forces required both for de-agglomeration of the powder bed and to overcome individual particle−particle adhesion (i.e., the critical pressure parameter) are investigated using conditions consistent with powder breakup during inhalation, namely under airflow.

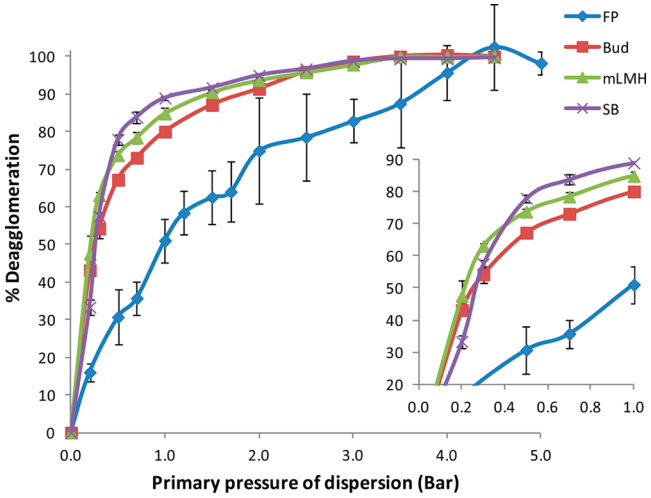

Figure 7. De-agglomeration profiles derived from particle size data generated by Sympatec HELOS/RODOS laser diffraction (using the rotary feeder) at primary pressures in the range 0.2−5.0 bar (inset is a magnification of the 0−1.0 bar region). Particle size data (i.e., DA_{50} values) were normalized using the D_m/D_x approach for the powders budesonide (Bud, red line), fluticasone propionate (FP1, blue line), lactohale 300 (mLac, green line), and salbutamol base (SB, purple line) (mean ± SD, $n = 3$). The data show the relative ease with which SB reaches full dispersion at a low airflow pressure drop. Bud and mLac undergo dispersion at low pressure drop values but require a higher pressure for full dispersion to be achieved. FP fails to disperse fully until high dispersion airflow is applied and exhibits heterogeneity in dispersibility.

The de-agglomeration analysis demonstrated the relative ease of de-agglomeration of SB and mLMH. More energy input was required to de-agglomerate Bud, and FP demonstrated very poor and heterogeneous de-agglomeration, indicating the presence of particles with high heterogeneity of agglomerate cohesion force. Following data normalization and linearization,[27] the linearity was found to be good for all powders (range for R^2 = 0.905−0.999). In accordance with previous analysis, the CPP, i.e., the pressure required to achieve 50% de-agglomeration (DA_{50}), was determined from the linear fit (Table 4).

Table 4. De-agglomeration Analysis of Pharmaceutical Powders Including Micronized and Coarse Active Pharmaceutical Ingredients and Excipients[a]

sample[b]	R^2	CPP (bar)	DA_{50} (bar)	FPF (%RD)	MMAD (μm)
SB	0.9979	1.0	0.25		
mLMH	0.9997	2.0	0.23		
Bud	0.9995	2.0	0.32		
FP1	0.9049	3.5	1.15		
mLMH (processed)	0.9897	1.2	0.07		
FP1 (processed)	0.9832	4.0	0.48	27.98 ± 2.95	4.40 ± 0.27
FP1−mLMH 1:5	0.9849	3.5	0.61	19.36 ± 2.38	4.76 ± 0.17
FP1−mLMH 1:6	0.9773	3.5	0.57	22.43 ± 4.18	4.73 ± 0.39
FP2−cLMH				7.95 ± 0.65	4.22 ± 0.07

[a]De-agglomeration analysis was performed by laser diffraction for micronized substances (derived parameters: critical primary pressure (CPP) and ease of de-agglomeration (DA_{50}); R^2 indicates linearity. Formulated blends (mean ± SD, $n \geq 3$) were assessed for de-agglomeration by inertial impaction (determined parameters: fine particle fraction (FPF < 5 μm) expressed as a percentage of the total recovered dose (RD) and mass median aerodynamic diameter (MMAD)) of micronized substances co-formulated in fine particle blends. [b]SB, micronized salbutamol base; mLMH, micronized lactose; Bud, micronized budesonide; FP, micronized fluticasone propionate; FP−mLMH, FP mixed with micronized lactose; FP2−cLMH, 1.8% FP with coarse lactose.

The results presented in Table 4 indicate a range of powder de-agglomeration behaviors. The CPP expresses the airflow pressure required to fully disperse the most cohesive agglomerates in the powder. It can be seen that SB represented the least cohesive powder and FP had the most cohesive agglomerates. The values of the DA_{50} suggest that SB, Bud, and mLMH all achieved effective dispersal at low airflow pressures

dx.doi.org/10.1021/mp500335w | Mol. Pharmaceutics 2015, 12, 18−33

(0.23−0.32 bar); however, both mLMH and Bud contained a population of agglomerates which required higher dispersion forces to achieve full de-agglomeration. FP represents a very cohesive powder which is dispersed into large agglomerates at low pressures (DA_{50} = 1.15 bar), and these agglomerates have high cohesive forces, requiring 3.0 bar airflow pressure for full de-agglomeration.

The rapid decrease in the aerosol median diameter for SB upon application of dispersing pressures and attainment of full de-agglomeration at low forces indicates low and homogeneous forces of SB−SB cohesion. Such observations are consistent with fluidization via an erosion mechanism, where a stream of de-agglomerated particles is continually entrained into the airflow, even at low flow rates.[48,49] A similar behavior was seen for Bud and mLMH, albeit with a greater heterogeneity in the Bud−Bud and mLMH−mLMH cohesive force distribution, as shown by the greater difference between DA_{50} and CPP values. The heterogeneity in the forces of inter-particulate interaction is clearly observable in the FP dispersion curves, with high standard deviations in the measured agglomerate sizes across the dispersing pressures for FP. This highlighted agglomerate size heterogeneity during dispersion indicates that, under a given level of shear, there will be mixed populations of large-to-medium-sized, highly cohesive agglomerates and de-agglomerated particles aerosolized from the powder bed.

The effect of a typical powder processing operation (tumbling/blending) was also assessed using powder de-agglomeration analysis. It can be seen that the tumbling of FP worsened the heterogeneity of cohesive interactions in the powder blend, which may be related to powder microstructure.[26] The lowering of the DA_{50} for FP indicated an improved aerosolization of an easily dispersed population of particles from the powder bed (i.e., more particles dispersed into individual particles and smaller agglomerates at lower airflow rates). However, the CPP remained high (4.0 bar), indicating the difficulty in dispersing the cohesive agglomerates into an aerosol of fully dispersed (individual) particles. For mLMH, the powder dispersed more readily, and the tumbling also served to disrupt the cohesive forces of the powder, leading to lower airflow forces required to disrupt even the most cohesive mLMH agglomerates.

4.5. Pre-screening Formulation Interactions through Adhesive Force Determination. In inhaled formulations, the balance of the cohesive to adhesive forces is crucial to the formulation performance in carrier-based blends. Frequently, mLMH is added to blends to alter the CAB. Therefore, it was of interest to examine the rapid screening ability of synthonic engineering and the powder dispersal approach to CABs. To use the synthonic approach to determine the adhesive strengths of FP with LMH, the APIs were treated as probe systems, and their interactions on eight surfaces of LMH are tabulated in Table 3. The strongest energy on each of these surfaces was recorded from the simulation. It is revealed in this table that the adhesive strengths of the APIs on all the LMH surfaces were very similar, and although FP−LMH adhesive strength was similar to the FP−FP cohesive strength, it was lower than the LMH−LMH cohesive strength.

Mixing FP with mLMH in two different proportions revealed an interesting behavior. The materials were blended with the intention to produce FP-rich and mLMH-rich blends; however, the actual FP:mLMH ratios determined during content uniformity testing were 1:5 and 1:6, indicating that mLMH-rich blends resulted. Upon analysis, a low DA_{50} was observed (indicating ready dispersal of the powder into an aerosol cloud), but a high CPP value was maintained, characteristic of FP on its own. This suggests that the addition of mLMH to FP was unable to disrupt the cohesive interactions of the FP agglomerates; rather, it only altered the bulk powder cohesion. Therefore, the aerosol that is formed is hypothesized to consist of agglomerates of FP which still require high airflow forces to de-agglomerate.

The latter findings are supported by the study of surface cohesion of FP by SEA. All samples of micronized material displayed heterogeneous surface energy distributions, and the dispersive component contributed to the major part of the total surface energy (data not presented). For means of comparison with the computational predictions, the surface energy values corresponding to a surface coverage of 0.01 n/n_m are presented (Table 5) in order to probe the highest energy surface sites on

Table 5. Dispersive Surface Energy, Specific Surface Energy, and Work of Cohesion or Adhesion for Inhalation Particles

sample[a]	dispersive surface energy (mJ/m^2)	specific surface energy (mJ/m^2)	work of cohesion/ adhesion (mJ/m^2)
FP1	47.9	6.3	108.6
mLMH	52.5	6.9	119.0
FP1−mLMH			113.7
FP2	42.8	5.8	97.2
cLMH	65.3	12.3	155.3
FP2−cLMH			123.2

[a]FP1, micronized fluticasone propionate (batch no. 458763, LGM Pharma); FP2, micronized fluticasone propionate (batch no. 5501-B-11030, LGM Pharma); mLMH, micronized lactose monohydrate (Lactohale LH300); cLMH, coarse-grade lactose monohydrate (batch no. 120904-25, Pfizer Global Research & Development).

the drug and excipient materials. The surface energy of mFP1 and mLMH both demonstrated predominantly dispersive components. The work of adhesion between the two materials was determined to be was ∼113.7 mJ/m^2 for mLMH−FP interactions. The findings suggest that the interaction energy between mLMH and FP would be insufficient to break-up the strongest mLMH cohesive interactions, and hence segregation into FP-rich and mLMH-rich blend regions was predicted. The surface of cLMH was more polar than that of mLMH and exhibited a work of cohesion of ∼155 mJ/m^2 for cLMH. The work of adhesion of FP2−cLMH was ∼123 mJ/m^2, indicating that, similar to blending with mLMH, FP particles are unlikely to form adhesive interactions with cLMH. The latter findings were in broad agreement with the aerosolization measurements of de-agglomeration (where addition of LMH to FP failed to break-up agglomerates during aerosolization, Table 4) and with the computational predictions (section 4.3). Although it is accepted that the probing of only the most energetic surface sites through the SEA is a reductionist approach, the concept is compatible with the "active site" hypothesis[50] of dry powder inhalation blend formation.

4.6. Aerosolization Analysis. A typical particle deposition profile for an FP blend following aerosolization at 60 L/min (or 1.4 kPa) into the next-generation impactor is shown in Figure 8 for the FP2−cLMH blend. The aerosolization performance for both the cLMH and mLMH blends presented in Table 4 indicates the lack of improvement in fine particle dispersion following blending of FP with lactose monohydrate. The fine

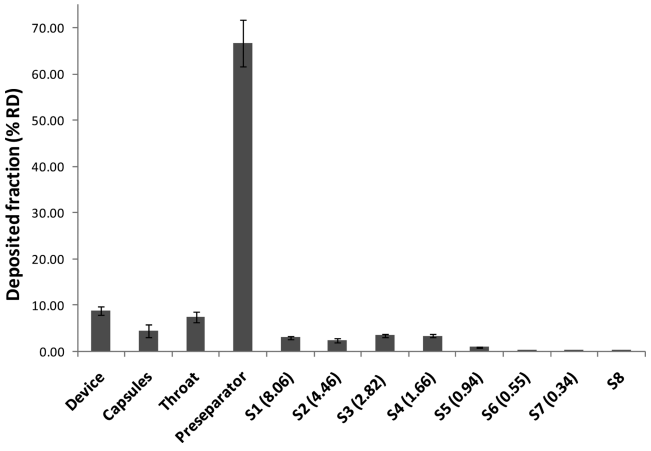

Figure 8. Deposition profile of fluticasone propionate in the next-generation impactor following aerosolization. S1−S8 indicate the stage number and respective aerodynamic cutoff diameter of the stage (in μm at 60 L/min). Data represent mean ± SD, $n = 3$. The formulation exhibits poor dispersion of FP into respirable particles (fraction depositing on stages 2−8). Instead, large drug aggregates and drug which remains adhered to the carrier lactose particles predominate (i.e., high pre-separator deposition).

particle fraction (FPF < 5 μm) for FP alone was low (~26%), and the dispersed particles possessed a large mass median aerodynamic diameter (~4.50 μm), with no statistically significant improvement in the dispersion upon blending with mLMH ($p > 0.05$, ANOVA and posthoc Tukey's test). Upon blending with coarse lactose, the FPF was considerably lower ($p < 0.05$) compared to that of FP alone; however, once more there was no significant decrease in the aerodynamic diameter. The deposition profile for FP2−cLMH blends (representative of a DPI product) showed a pronounced pre-separator deposition fraction as well as a high MMAD value. This suggests the aerosolization of large agglomerates of the drug and/or the poor removal of surface-adhered FP particles. A scanning electron micrograph of the FP2−cLMH blend before aerosolization (Figure 9) supports that argument, with large agglomerates as well as some individual identifiable particles stuck to the surface of the carrier particle. In order to achieve a high FPF, both agglomerates and individual drug particles would need to be removed from the carrier surface by aerodynamic shear forces and impaction within the device. However, poor de-agglomeration owing to the high cohesive force distribution for the FP−FP interactions would lead to inefficient de-agglomeration and persistence of the high MMAD, even following blending with the carrier.

5. APPLICABILITY AND LIMITATIONS OF THE RAPID PREDICTION FORMULATION ENGINEERING APPROACHES

The use of an atom−atom systematic search computational approach has proved powerful for the *in silico* prediction of cohesive forces of pharmaceutical powders. A rank-order correlation was achieved with experimental determination of de-agglomeration under airflow dispersion in the case of micronized particles of APIs, where surface energies were found to be dominated by non-polar van der Waals dispersion forces. The computational modeling of LMH surface energy predicted a substantially higher cohesive force than any of the APIs, which was not in keeping with the powder dispersal analysis for mLMH. Furthermore, although the modeling approach predicted FP to have an adhesively balanced interaction with LMH, the prediction was not verified by experimental observations using powder dispersal (Table 4) or SEA characterization for mLMH. Reports have suggested that FP has adhesive interactions with LMH in dry powder formulations.[51] However, researchers from the same group have also shown, when performing functional performance

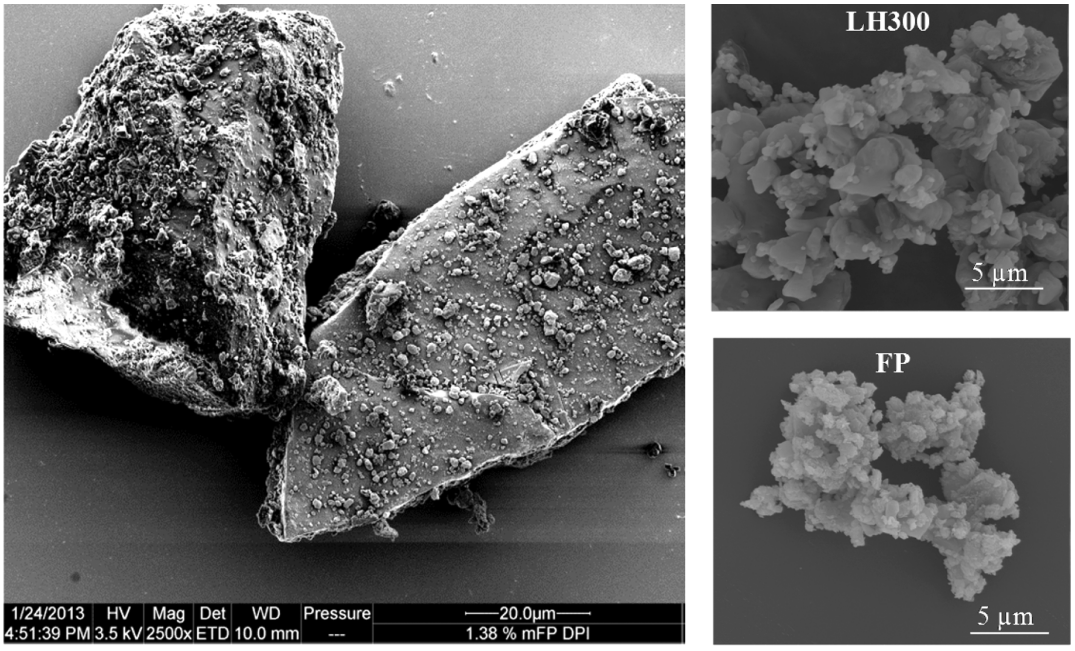

Figure 9. Scanning electron microscopy images of a 1.38% w/w dry powder blend of fluticasone propionate with coarse lactose monohydrate (left), micronized lactose (LH300), and micronized fluticasone propionate (FP). FP agglomerates and individual FP particles are visible on the surface of the coarse carrier lactose.

dx.doi.org/10.1021/mp500335w | *Mol. Pharmaceutics* 2015, 12, 18−33

testing, that the cohesive agglomeration of FP within a formulation depends critically on the processing history of the micronized powder.[10] In our experimental analysis with FP2 and cLMH, SEA incorporating polar probes indicated that an adhesive FP−cLMH interaction would be sufficient to disrupt cohesive FP−FP interactions but not cLMH−cLMH interactions. It is therefore appropriate to consider several points:

- the behavior of powders compared to individual particles;
- the limitations of the surface energy by experimental determination in the current report; and
- the assumptions of the synthonic engineering approach.

When formulating powders suitable for inhalation, the high specific surface area of the micrometer-sized particles results in particles cohering together (e.g., Figure 9). Cohesion may be aided by surface activation of the powders due to milling.[18,52] Therefore, the principal interest during formulation is in disrupting the cohesive agglomerates to ensure (a) aerosolization or (b) interactive mixing with formulation components. With respect to aerosolization, excellent agreement was observed between the dispersal analysis of principally nonpolar compounds and the synthonic modeling predictions. However, assessment of the polar LMH was found to correlate poorly to the functional measurements, and indeed LMH was predicted to be the most cohesive of materials studied. It should be borne in mind that the powders consist of collections of agglomerates which interact with inter-agglomerate adhesion forces, as well as inter-particulate interactions within the agglomerates.[23] Therefore, although the synthonic modeling approach applied in this study assumes unhindered surface contact between the probe molecule and a crystal surface, this situation is unlikely to exist in the more representative case of a practical powder system, where the exact topochemical alignment between API and the mLMH excipient, despite its higher interaction energy, might be less favored statistically when considered in competition with the more stochastic isotropic dispersive interactions. In addition, the intra-agglomerate and inter-agglomerate porosity (sensitive to particle density, shape, charge, and size distribution, including the presence of "fine lactose" which reduced carrier−carrier cohesive forces) will also play a role in the cohesion process through its dictation of the extent of cohering contact points and permeability to the dispersing airflow,[48] respectively. Therefore, although the cohesion of LMH is predicted to be highest, this would require the highest energy sites to be closely aligned with each other either within the particles or the agglomerate. Mindful of the anomaly with respect to the polar mLMH, an alternative approach would be to use the more computational demanding surface−surface systematic approach,[32,33] through which the energy landscape between two surfaces can be probed and the assumption inherent in the molecule−surface modeling removed. If the above supposition were to be true, then a much sharper interaction minimum would be expected in the case of mLMH when compared to the APIs. Further work is planned to test this supposition.

SEA of LMH and FP correlated well to the predictions in terms of ranking of cohesive and adhesive forces, with cLMH found to have the highest cohesive interaction of all materials tested when polar probes were included. However, the polar contribution of LMH is profoundly affected by the presence of surface moisture,[47] which the IGC data could not take into account since it was performed at 0% RH. It was appropriate for the purposes of the current study to consider surface energy distributions at 0% RH for effective comparison with the synthonic modeling approaches. The presence of water vapor can contribute to the magnitude of cohesive (and adhesive) interactions under in-use conditions of many lactose-based formulations.[53] All aerosolization studies were performed with RH < 50%, at which the adsorption of water vapor to FP surfaces is low[54] and unexpected to alter cohesion forces. Furthermore, although mLMH is susceptible to surface adsorption and condensation of water vapor, previous studies have shown no impact of RH < 65% on blends of FP with cLMH.[55] In developing the rapid prediction tools further, it will be important to perform SEA at a range of RH levels as well as to incorporate surface capillary moisture interactions in synthonic modeling. It is also important to consider that powders for inhalation demonstrate heterogeneity of surface energy distributions. By probing only the highest surface energy sites using low surface coverage methods,[56] an unrealistic indication of the forces of interaction will be determined. For example, the highest energy FP surface sites may well be able to adhere to the lowest energy cLMH sites, but they would be unlikely to disrupt the most cohesive of cLMH interactions. Thus, it can be seen in Figure 9 that FP particles have indeed adhered as individual particles to several sites on the lactose carrier particle. Because the blending process employed was a low-shear process, it is unlikely that cohesive agglomerates of FP2 starting material would have been disrupted to enable the FP−cLMH adhesion to occur. Assuming similar energy distributions for mLMH and cLMH (i.e., including polar surface energy), it is unlikely that low shear tumbling would be sufficient to disrupt mLMH−mLMH (or cLMH−cLMH) and FP−FP interactions to facilitate the FP−LMH interactions that were predicted to be favorable from the synthonic modeling calculations. The latter discussion is supported by impaction analysis, where the lack of a change in MMAD when FP was blended with an excess of mLMH or cLMH demonstrated the existence of cohesive FP agglomerates in the blends.

6. CONCLUSIONS

The ability of the synthonic modeling approach to provide a molecular-level understanding of the surface properties of inhalation powders was demonstrated by assessing the cohesivity of three active pharmaceutical ingredients (API, fluticasone propionate (FP), budesonide (Bud), and salbutamol base (SB)) and the commonly used excipient, α-lactose monohydrate (LMH). The predictions showed that FP (−11.5 kcal/mol) has the highest cohesive strength when compared to Bud (−9.9 kcal/mol) or SB (−7.8 kcal/mol), and this prediction of cohesive strength ranking validates well the cohesive strength measurements using laser diffraction from the airflow pressure required for complete dispersion (CPP), which were 3.5, 2.0, and 1.0 bar for FP, Bud, and SB, respectively. The highest cohesive strength, as predicted for LMH (−15.9 kcal/mol), did not correlate with the experimental CPP value of 2.0 bar (i.e., ranking lower than FP), and this can be attributed mainly to the presence of water and hydroxyl groups in lactose, which lead to very high electrostatic and H-bond components of the cohesive energy, unlike in the APIs. A direct comparison of the predicted and measured cohesive balance of LMH with APIs will require a more in-depth understanding of highly hydrogen-bonded systems using the synthonic engineering modeling tools, In addition the application of a more

computationally intense surface−surface systematic approach will be required.

Despite the limiting assumptions of the synthonic modeling approach, it has proved a powerful characterization tool for predicting inter-particulate interactions in the practical powder systems important in drug product formulation. The correlation of the predicted cohesive rank order with the functional dispersal assessment for the non-polar APIs was promising. In addition, in a carrier-based lactose blend, similar predictions of adhesive potential for FP−cLMH were made using the synthonic modeling calculations and infinite dilution IGC incorporating polar and non-polar probe gases. It has not escaped our attention that synthonic modeling could have utility in drug product formulation design; in particular, they could be used to guide excipient choice and processing conditions (e.g., high versus low shear blending) and to predict consistency of performance in the development of high-quality and low-variability drug products using a quality-by-design approach.

■ ASSOCIATED CONTENT

Supporting Information

Additional figures showing predicted morphologies of Bud and SB, and surface chemistry of LMH, FP, Bud, and SB surfaces. This material is available free of charge via the Internet at http://pubs.acs.org.

■ AUTHOR INFORMATION

Corresponding Authors

*Darragh Murnane, E-mail d.murnane@herts.ac.uk, phone +044 1707 285904.

* Kevin J. Roberts, E-mail k.j.roberts@leeds.ac.uk, phone +044 113 34 35836

Notes

The authors declare no competing financial interest.

■ ACKNOWLEDGMENTS

We are most grateful to Pfizer for their current and most generous support of Synthonic Engineering research at Leeds. This research area was initiated through an EPSRC Follow-on grant (EP/I028293/1) in collaboration with CCDC, Infineum, Malvern Instruments, Nexia Solutions, Pfizer, and Syngenta, to whom we are most grateful. The authors acknowledge the financial support from BBSRC Doctoral Training Award (BB/F017626/1) and Pfizer Global R&D for the financial support of S.J. We are also grateful to Dr. Jiyi Khoo, Dr. Majid Naderi, and Surface Measurement Systems Ltd. (UK) for supporting the gas chromatography studies.

■ REFERENCES

(1) Hooton, J. C.; Jones, M. D.; Price, R. Predicting the behavior of novel sugar carriers for dry powder inhaler formulations via the use of a cohesive-adhesive force balance approach. *J. Pharm. Sci.* **2006**, *95* (6), 1288−1297.

(2) Begat, P.; Morton, D. A. V.; Staniforth, J. N.; Price, R. The Cohesive-Adhesive Balances in Dry Powder Inhaler Formulations 1: Direct Quantification by Atomic Force Microscopy. *Pharm. Res.* **2004**, *21* (9), 1591−1597.

(3) Arlin, J.-B.; Price, L. S.; Price, S. L.; Florence, A. J. A strategy for producing predicted polymorphs: catemeric carbamazepine form V. *Chem. Commun.* **2011**, *47* (25), 7074−7076.

(4) Li, Q.; Rudolph, V.; Weigl, B.; Earl, A. Interparticle van der Waals force in powder flowability and compactibility. *Int. J. Pharm.* **2004**, *280* (1−2), 77−93. Wang, J. J.; Li, T. L.; Bateman, S. D.; Erck, R.; Morris, K. R. Modeling of adhesion in tablet compression - I. Atomic force microscopy and molecular simulation. *J. Pharm. Sci.* **2003**, *92* (4), 798−814.

(5) Saxena, A.; Kendrick, J.; Grimsey, I. M.; Roberts, R.; York, P. A combined modelling and experimental study of the surface energetics of α-lactose monohydrate. *J. Pharm. Sci.* **2010**, *99* (2), 741−752.

(6) Liltorp, K.; Larsen, T. G.; Willumsen, B.; Holm, R. Solid state compatibility studies with tablet excipients using non thermal methods. *J. Pharm. Biomed. Anal.* **2011**, *55* (3), 424−428.

(7) Yu, L. X. Pharmaceutical quality by design: Product and process development, understanding, and control. *Pharm. Res.* **2008**, *25* (10), 2463−2463.

(8) Kaialy, W.; Alhalaweh, A.; Velaga, S. P.; Nokhodchi, A. Effect of carrier particle shape on dry powder inhaler performance. *Int. J. Pharm.* **2011**, *421* (1), 12−23.

(9) Hickey, A. J.; Mansour, H. M.; Telko, M. J.; Xu, Z.; Smyth, H. D. C.; Mulder, T.; McLean, R.; Langridge, J.; Papadopoulos, D. Physical characterization of component particles included in dry powder inhalers. II. Dynamic characteristics. *J. Pharm. Sci.* **2007**, *96* (5), 1302−1319.

(10) Kubavat, H. A.; Shur, J.; Ruecroft, G.; Hipkiss, D.; Price, R. Investigation into the Influence of Primary Crystallization Conditions on the Mechanical Properties and Secondary Processing Behaviour of Fluticasone Propionate for Carrier Based Dry Powder Inhaler Formulations. *Pharm. Res.* **2012**, *29* (4), 994−1006.

(11) Hickey, A. J.; Mansour, H. M.; Telko, M. J.; Xu, Z.; Smyth, H. D. C.; Mulder, T.; McLean, R.; Langridge, J.; Papadopoulos, D. Physical characterization of component particles included in dry powder inhalers. I. Strategy review and static characteristics. *J. Pharm. Sci.* **2007**, *96* (5), 1282−1301.

(12) Usmani, O. S.; Biddiscombe, M. F.; Barnes, P. J. Regional lung deposition and bronchodilator response as a function of beta(2)-agonist particle size. *Am. J. Respiratory Crit. Care Med.* **2005**, *172* (12), 1497−1504.

(13) Adi, S.; Adi, H.; Chan, H.-K.; Finlay, W. H.; Tong, Z.; Yang, R.; Yu, A. Agglomerate strength and dispersion of pharmaceutical powders. *J. Aerosol Sci.* **2011**, *42* (4), 285−294.

(14) Louey, M. D.; Van Oort, M.; Hickey, A. J. Aerosol dispersion of respirable particles in narrow size distributions using drug-alone and lactose-blend formulations. *Pharm. Res.* **2004**, *21* (7), 1207−1213. Chow, A. H. L.; Tong, H. H. Y.; Chattopadhyay, P.; Shekunov, B. Y. Particle engineering for pulmonary drug delivery. *Pharm. Res.* **2007**, *24* (3), 411−437. Telko, M. J.; Hickey, A. J. Dry powder inhaler formulation. *Respir. care* **2005**, *50* (9), 1209−1227. Jones, M. D.; Santo, J. G. F.; Yakub, B.; Dennison, M.; Master, H.; Buckton, G. The relationship between drug concentration, mixing time, blending order and ternary dry powder inhalation performance. *Int. J. Pharm.* **2010**, *391* (1−2), 137−147.

(15) Lohrmann, M.; Kappl, M.; Butt, H.-J.; Urbanetz, N. A.; Lippold, B. C. Adhesion forces in interactive mixtures for dry powder inhalers - Evaluation of a new measuring method. *Eur. J. Pharm. Biopharm.* **2007**, *67* (2), 579−586.

(16) Hooton, J. C.; Jones, M. D.; Harris, H.; Shur, J.; Price, R. The influence of crystal habit on the prediction of dry powder inhalation formulation performance using the cohesive-adhesive force balance approach. *Drug Dev. Ind. Pharm.* **2008**, *34* (9), 974−983. Jones, M. D.; Price, R. The influence of fine excipient particles on the performance of carrier-based dry powder inhalation formulations. *Pharm. Res.* **2006**, *23* (8), 1665−1674. Jones, M. D.; Harris, H.; Hooton, J. C.; Shur, J.; King, G. S.; Mathoulin, C. A.; Nichol, K.; Smith, T. L.; Dawson, M. L.; Ferrie, A. R.; Price, R. An investigation into the relationship between carrier-based dry powder inhalation performance and formulation cohesive-adhesive force balances. *Eur. J. Pharm. Biopharm.* **2008**, *69* (2), 496−507.

(17) James, J.; Crean, B.; Davies, M.; Toon, R.; Jinks, P.; Roberts, C. J. The surface characterisation and comparison of two potential sub-micron, sugar bulking excipients for use in low-dose, suspension

formulations in metered dose inhalers. *Int. J. Pharm.* **2008**, *361* (1−2), 209−221.
(18) Feeley, J. C.; York, P.; Sumby, B. S.; Dicks, H. Determination of surface properties and how characteristics of salbutamol sulphate, before and after micronisation. *Int. J. Pharm.* **1998**, *172* (1−2), 89−96.
(19) Ticehurst, M. D.; Basford, P. A.; Dallman, C. I.; Lukas, T. M.; Marshall, P. V.; Nichols, G.; Smith, D. Characterisation of the influence of micronisation on the crystallinity and physical stability of revatropate hydrobromide. *Int. J. Pharm.* **2000**, *193* (2), 247−259. Ticehurst, M. D.; Rowe, R. C.; York, P. Determination of the Surface-Properties of 2 Batches of Salbutamol Sulfate by Inverse Gas-Chromatography. *Int. J. Pharm.* **1994**, *111* (3), 241−249.
(20) Gamble, J. F.; Leane, M.; Olusanmi, D.; Tobyn, M.; Supuk, E.; Khoo, J.; Naderi, M. Surface energy analysis as a tool to probe the surface energy characteristics of micronized materials-A comparison with inverse gas chromatography. *Int. J. Pharm.* **2012**, *422* (1−2), 238−244.
(21) Gamble, J. F.; Dave, R. N.; Kiang, S.; Leane, M. M.; Tobyn, M.; Wang, S. S. Y. Investigating the applicability of inverse gas chromatography to binary powdered systems: An application of surface heterogeneity profiles to understanding preferential probe-surface interactions. *Int. J. Pharm.* **2013**, *445* (1−2), 39−46.
(22) Tong, H. H. Y.; Shekunov, B. Y.; York, P.; Chow, A. H. L. Predicting the aerosol performance of dry powder inhalation formulations by interparticulate interaction analysis using inverse gas chromatography. *J. Pharm. Sci.* **2006**, *95* (1), 228−233. Shekunov, B. Y.; Feeley, J. C.; Chow, A. H. L.; Tong, H. H. Y.; York, P. Aerosolisation behaviour of micronised and supercritically-processed powders. *J. Aerosol Sci.* **2003**, *34* (5), 553−568. Davies, M.; Brindley, A.; Chen, X. Y.; Marlow, M.; Doughty, S. W.; Shrubb, I.; Roberts, C. J. Characterization of drug particle surface energetics and Young's modulus by atomic force microscopy and inverse gas chromatography. *Pharm. Res.* **2005**, *22* (7), 1158−1166. Marsac, P. J.; Shamblin, S. L.; Taylor, L. S. Theoretical and practical approaches for prediction of drug-polymer miscibility and solubility. *Pharm. Res.* **2006**, *23* (10), 2417−2426.
(23) Das, S. C.; Behara, S. R. B.; Bulitta, J. B.; Morton, D. A. V.; Larson, I.; Stewart, P. J. Powder Strength Distributions for Understanding De-agglomeration of Lactose Powders. *Pharm. Res.* **2012**, *29* (10), 2926−2935.
(24) Saleem, I.; Smyth, H.; Telko, M. Prediction of dry powder inhaler formulation performance from surface energetics and blending dynamics. *Drug Dev. Ind. Pharm.* **2008**, *34* (9), 1002−1010.
(25) Murnane, D.; Martin, G. P.; Marriott, C. Investigations into the Formulations of Metered Dose Inhalers of for Inhalation of Salmeterol Xinafoate and Fluticasone Propionate Microcrystals. *Pharm. Res.* **2008**, *25* (10), 2283−2291.
(26) Behara, S. R. B.; Larson, I.; Kippax, P.; Morton, D. A. V.; Stewart, P. An approach to characterising the cohesive behaviour of powders using a flow titration aerosolisation based methodology. *Chem. Eng. Sci.* **2011**, *66* (8), 1640−1648.
(27) Jaffari, S.; Forbes, B.; Collins, E.; Barlow, D. J.; Martin, G. P.; Murnane, D. Rapid characterisation of the inherent dispersibility of respirable powders using dry dispersion laser diffraction. *Int. J. Pharm.* **2013**, *447* (1−2), 124−131.
(28) Parisini, I.; Murnane, D. Iterative Mathematical Approach for understanding deagglomeration behaviour of micronized cohesive powder in formulations, Presented at Drug Delivery to the Lungs - DDL24 Conference, Edinburgh, Dec 11−13, 2013; The Aerosol Society: North Somerset, UK, 2013
(29) Price, S. L. Predicting crystal structures of organic compounds. *Chem. Soc. Rev.* **2014**, *43*, 2098−2111.
(30) Anuar, N.; Daud, W. R. W.; Hammond, R. B.; Roberts, K. J.; Kamarudin, S. K.; Tasirin, S. M. Morphology and associated surface chemistry of L-iosleucine crystals modelled under the influence of L-leucine additive molecules. *Cryst. Growth Des* **2012**, *12* (5), 2195−2203. Clydesdale, G.; Hammond, R. B.; Roberts, K. J. Molecular modeling of bulk impurity segregation and impurity-mediated crystal habit modification of naphthalene and phenanthrene in the presence of heteroimpurity species. *J. Phys. Chem. B* **2003**, *107* (20), 4826−4833. Hammond, R. B.; Ramachandran, V.; Roberts, K. J. Molecular modeling of the incorporation of habit modifying additive:alpha-glycine in the presence of L-alanine. *CrystEngComm* **2011**, *13* (15), 4935−4944. Hammond, R. B.; Pencheva, K.; Roberts, K. J. A structural-kinetic approach to model face-specific solution/crystal surface energy associated with the crystallization of acetyl salicylic acid from supersaturated aqueous/ethanol solution. *Cryst. Growth Des.* **2006**, *6* (6), 1324−1334.
(31) Hammond, R. B.; Ma, C.; Roberts, K. J.; Ghi, P. Y.; Harris, R. K. Application of systematic search methods to studies of the structures of urea-dihydroxy benzene cocrystals. *J. Phys. Chem. B* **2003**, *107* (42), 11820−11826. Hammond, R. B.; Hashim, R. S.; Ma, C.; Roberts, K. J. Grid-based molecular modeling for pharmaceutical salt screening: Case example of 3,4,6,7,8,9-hexahydro-2H-pyrimido (1,2-a) pyrimidinium acetate. *J. Pharm. Sci.* **2006**, *95* (11), 2361−2372.
(32) Hammond, R. B.; Pencheva, K.; Roberts, K. J. Simulation of energetic stability of facetted L-glutamic acid nanocrystalline clusters in relation to their polymophic phase stabilityas a funciton of crysal size. *J. Phys. Chem. B* **2005**, *109* (42), 19550−19552.
(33) Hammond, R. B.; Jeck, S.; Ma, C. Y.; Pencheva, K.; Roberts, K. J.; Auffret, T. An Examination of Binding Motifs Associated With Inter-Particle Interactions between Facetted Nano-Crystals of Acetylsalicylic Acid and Ascorbic Acid through the Application of Molecular Grid-Based Search Methods. *J. Pharm. Sci.* **2009**, *98* (12), 4589−4602.
(34) Hammond, R. B.; Roberts, K. J.; Smith, E. D. L.; Docherty, R. Application of a computational systematic search strategy to study polymorphism in phenazine and perylene. *J. Phys. Chem. B* **1999**, *103* (37), 7762−7770. Hammond, R. B.; Pencheva, K.; Roberts, K. J. Molecular modeling of crystal-crystal interactions between the alpha- and beta-polymorphic forms of L-glutamic acid using grid-based methods. *Cryst. Growth Des.* **2007**, *7* (5), 875−884. Hammond, R. B.; Pencheva, K.; Roberts, K. J. An examination of polymorphic stability and molecular conformational flexibility as a function of crystal size associated with the nucleation and growth of benzophenone. *Faraday Discuss.* **2007**, *136*, 91−106.
(35) Smith, J. H.; Dann, S. E.; Elsegood, M. R. J.; Dale, S. H.; Blatchford, C. F. α-lactose monohydrate: a redetermination at 150 K. *Acta Crystallogr. Sect. E: Struct. Rep.Online* **2005**, *61* (8), o2499−o2501.
(36) Beale, J. P.; Stephenson, N. C. X-Ray Analysis of Th 1165a and Salbutamol. *J. Pharm. Pharmacol.* **1972**, *24* (4), 277−280.
(37) Cejka, J.; Kratochvil, B.; Jegorov, A. Crystal structure of fluticasone propionate, C25H31F3O5S. *Z. Kristallogr.—New Cryst. Struct.* **2005**, *220* (2), 143−144.
(38) Albertsson, J.; Oskarsson, A.; Svensson, C. X-ray study of Budesonide - Molecular-structure and solid-solution of (22S) and (22R) epimers of11-beta,21-dihydroxy-16-alpha,17-alpha-propylmethylenedioxy-1,4-pregnadiene-3,20-dione. *Acta Crystallogr. Sect. B—Struct. Sci.* **1978**, *34* (Oct), 3027−3036.
(39) Clydesdale, G.; Roberts, K. J.; Docherty, R. HABIT95—A program for predicting the morphology of molecular crystals as a function of growth environment. *J. Cryst. Growth* **1996**, *166* (1−4), 78−83. Roberts, K. J.; Walker, E. M.; Clydesdale, G. *The Crystal Habit of Molecular Materials: A Structural Perspective, In Theoretical aspects and computer modelling of the molecular solid state*; John Wiley & Sons: New York, 1996.
(40) Clydesdale, G.; Thomson, G. B.; Walker, E. M.; Roberts, K. J.; Meenan, P.; Docherty, R. A molecular modelling study of the crystal morphology of adipic acid and its habit modification by homologous impurities. *Cryst. Growth Des.* **2005**, *5* (6), 2154−2163.
(41) *Materials Studio*, 6.0; Accelrys Software Inc., 2011.
(42) Mayo, S. L.; Olafson, B. D.; Goddard, W. A. Dreiding - a Generic Force-Field for Molecular Simulations. *J. Phys. Chem.* **1990**, *94* (26), 8897−8909.
(43) Schultz, J.; Lavielle, L.; Martin, C. The Role of the Interface in Carbon Fibre-Epoxy Composites. *J. Adhes.* **1987**, *23* (1), 45−60.
(44) Traini, D.; Young, P. M.; Thielmann, F.; Acharya, M. The influence of lactose pseudopolymorphic form on salbutamol sulfate-

lactose interactions in DPI formulations. *Drug Dev. Ind. Pharm.* **2008**, *34* (9), 992−1001.
(45) Murnane, D.; Martin, G. P.; Marriott, C. Dry Powder Formulations for Inhalation of Fluticasone Propionate and Salmeterol Xinafoate Microcrystals. *J. Pharm. Sci.* **2009**, *98* (2), 503−515.
(46) *Mercury CSD 3.1.1*, v 5.34; Cambridge Crytallographic Data Centre, Cambridge, 2013.
(47) Das, S.; Larson, I.; Young, P.; Stewart, P. Understanding lactose behaviour during storage by monitoring surface energy change using inverse gas chromatography. *Dairy Sci. Technol.* **2010**, *90* (2−3), 271−285.
(48) Shur, J.; Harris, H.; Jones, M. D.; Kaerger, J. S.; Price, R. The role of fines in the modification of the fluidization and dispersion mechanism within dry powder inhaler formulations. *Pharm. Res.* **2008**, *25* (7), 1631−1640.
(49) Tuley, R.; Shrimpton, J.; Jones, M. D.; Price, R.; Palmer, M.; Prime, D. Experimental observations of dry powder inhaler dose fluidisation. *Int. J. Pharm.* **2008**, *358* (1−2), 238−247.
(50) Louey, M. D.; Stewart, P. J. Particle interactions involved in aerosol dispersion of ternary interactive mixtures. *Pharm. Res.* **2002**, *19* (10), 1524−1531.
(51) Young, P. M.; Price, R.; Jones, S.; Billings, M.-P. Investigation into drug and excipient interaction in dry powder inhaler combination products. *Respiratory Drug Delivery IX*, Vol. 3; Virginia Commonwealth University: Richmond, VA, 2004; 749−751.
(52) Brodka-Pfeiffer, K.; Langguth, P.; Grass, P.; Hausler, H. Influence of mechanical activation on the physical stability of salbutamol sulphate. *Eur. J. Pharm. Biopharm.* **2003**, *56* (3), 393−400. Le, V. N. P.; Robins, E.; Flament, M. P. Agglomerate behaviour of fluticasone propionate within dry powder inhaler formulations. *Eur. J. Pharm. Biopharm.* **2012**, *80* (3), 596−603.
(53) Price, R.; Young, P. M.; Edge, S.; Staniforth, J. N. The influence of relative humidity on particulate interactions in carrier-based dry powder inhaler formulations. *Int. J. Pharm.* **2002**, *246* (1−2), 47−59.
(54) Murnane, D.; Marriott, C.; Martin, G. P. Crystallization and crystallinity of fluticasone propionate. *Cryst. Growth Des.* **2008**, *8* (8), 2753−2764.
(55) Le, V. N. P.; Thi, T. H. H.; Robins, E.; Flament, M. P. Dry powder inhalers: Study of the parameters influencing adhesion and dispersion of fluticasone propionate. *AAPS PharmSciTech* **2012**, *13* (2), 477−484.
(56) Ho, R.; Muresan, A. S.; Hebbink, G. A.; Heng, J. Y. Y. Influence of fines on the surface energy heterogeneity of lactose for pulmonary drug delivery. *Int. J. Pharm.* **2010**, *388* (1−2), 88−94.